BBA - Biomembranes 1862 (2020) 183413

Contents lists available at ScienceDirect

BBA - Biomembranes

journal homepage: www.elsevier.com/locate/bbamem

Aggregation of 25-hydroxycholesterol in a complex biomembrane. Differences with cholesterol

Vicente Galiano[a], José Villalaín[b,*]

[a] Computers Engineering Department, Development, and Innovation in Healthcare Biotechnology (IDiBE), Universidad "Miguel Hernández", E-03202 Elche-Alicante, Spain
[b] Molecular and Cellular Biology Institute (IBMC) and Institute of Research, Development, and Innovation in Healthcare Biotechnology (IDiBE), Universidad "Miguel Hernández", E-03202 Elche-Alicante, Spain

ARTICLE INFO

Keywords:
25-Hydroxycholesterol
Late endosome membrane
Plasma membrane
Bis(monoacylglycero)phosphate
Cholesterol

ABSTRACT

25-Hydroxycholesterol (25HC), one of the most important oxysterol molecules, can be used by cells to fight bacterial and viral infections but the mechanism that defines its biological effects are unknown. Using molecular dynamics, we have aimed to describe the orientation and location of 25HC in the membrane as well as the interactions it might have with lipids. We have studied two complex model membrane systems, one similar to the late endosome membrane and the other one to the plasma membrane. Our results reinforce that 25HC is inserted in the membrane in a relative stable location similar to but not identical to cholesterol. 25HC fluctuates in the membrane to a much greater degree than cholesterol, but the effect of 25HC on the phospholipid order parameters is not significantly different. One of the most notable facts about 25HC is that, unlike cholesterol, this molecule tends to aggregate, forming dimers, trimers and higher-order aggregates. These aggregates are formed spontaneously through the formation of hydrogen bonds between the two 25HC atoms, the formation of hydrogen bonds being independent of the studied system. Remarkably, no contacts or hydrogen bonds are observed between 25HC and cholesterol molecules, as well as between cholesterol molecules themselves at any time. It would be conceivable that 25HC, by forming high order aggregates without significantly altering the membrane properties, would modify the way proteins interact with the membrane and henceforth form a true innate antiviral molecule.

1. Introduction

Cholesterol (CHOL) is an essential molecule for eukaryotic cells and their membranes, modulating various physical properties of the lipid bilayer such as fluidity and permeability [1]. CHOL is likely to interact with sphingomyelin and saturated phospholipids, forming liquid-ordered phases that coexist with liquid-disordered ones in the biological membrane [2]. Oxysterols are oxidized derivatives of CHOL produced by different processes, enzymatic and non-enzymatic, that have many different biological activities ~~by~~ either modulating the function of proteins or the physical properties of the membranes or both [3,4]. 25-Hydroxycholesterol (25HC), one of the most representative oxysterols, is enzymatically synthesized from CHOL by specific cholesterol-hydroxylases [5,6] (Supplementary Fig. 1F and G). 25HC, similarly to other oxysterols, has been known to regulate CHOL concentration in the membrane [7]. Interestingly, these enzymes are specifically expressed in macrophages and dendritic cells upon bacterial or viral infections, so that 25HC synthesis could be directly related to the immune system [7–9]. 25HC appears to play an important role in the regulation of CHOL homeostasis and the innate immune response [10,11]. However, it has been shown to be very effective in the inhibition of the cellular entry and replication of many different types of viruses, both enveloped and non-enveloped [5,12–17], so that this molecule has recently attracted the attention of numerous researchers. The recent outbreak of SARS-CoV-2 as well as any future viral outbreaks, which surely will happen, pose a serious global health risk and the search for effective antivirals is greater than ever [18].

25HC is able of inhibiting the replication of different enveloped

Abbreviations: BMP, bis(monoacylglycero)phosphate (sn-(3-oleoyl-2-hydroxy)-glycerol-1-phospho-sn-1′-(3′-oleoyl-2′-hydroxy)-glycerol); 25HC, 25-hydroxycholesterol; CHOL, cholesterol; LEM, late endosome membrane; PM, plasma membrane; POPC, 1-palmitoyl-2-oleoyl-sn-glycero-3-phosphocholine; POPE, 1-palmitoyl-2-oleoyl-sn-glycero-3-phosphoethanolamine; PI-3P, 1-palmitoyl-2-oleoyl-sn-glycero-3-phosphoinositol-3-phosphate; POPS, 1-palmitoyl-2-oleoyl-sn-glycero-3-phospho-L-serine

* Corresponding author at: Institute of Research, Development, and Innovation in Healthcare Biotechnology (IDiBE), Universitas "Miguel Hernández", E-03202 Alicante, Spain.
E-mail address: jvillalain@umh.es (J. Villalaín).

https://doi.org/10.1016/j.bbamem.2020.183413
Received 13 May 2020; Received in revised form 13 July 2020; Accepted 14 July 2020
Available online 25 July 2020

viruses, suggesting that it blocks the fusion between the viral and cellular [5]. More recently, it has also been shown that 25HC can inhibit HIV entry by directly blocking the fusion through the modulation of the biophysical properties of the membrane [19]. The capacity of 25HC of blocking both Zika virus infection and HCV replication by direct interaction with the membrane has also been demonstrated [14,20]. 25HC inhibits both DNA and RNA, enveloped and non-enveloped viruses and the list of different viruses inhibited by 25HC is growing in the literature [21–25]. Since 25HC has shown antiviral effects against many different types of viruses, it would be possible that it might interact with particular components of the biological membrane hampering the viral fusion course. Remarkably, the characteristic anionic lipid bis(monoacylglycero)phosphate (s-s 2,2′-dioleoyl lysobisphosphatidic acid, BMP) (Supplementary Fig. 1E) is only found in the membranes of late endosomes in a high concentration, where it seems to play an essential role in endosome function and dynamics as well as it seems a necessary requirement for viral membrane fusion [26–28]. Therefore, 25HC biological properties could be also attributed to its capability to interact with membrane lipids, as well as its ability to modify the biophysical properties of the membrane. In this perspective, it should be borne in mind that the concentration of 25HC found in the blood of healthy individuals is very low (nanomolar range) [29]. However, cellular treatment of 25HC as high as 5 μM showed significant inhibition of replication of a large number of viruses without any induction of cytotoxicity [25]. Therefore, information on the mechanism of action of 25HC might open up new opportunities for upcoming biomedical advances.

The only difference between CHOL and 25HC is the hydroxylation of carbon C25 of CHOL, change that reduces the hydrophobicity of the parent molecule and dramatically transforms 25HC into a bioactive molecule. Due to its hydrophobic character and its high phospholipid/water partition coefficient, 25HC possible effects on biological systems must be attributed to its ability to locate itself in the biological membrane and possibly change the membrane structure and dynamics [30,31]. The octanol/water partition XLogP3 value [32] of 25HC (6.8) is lower than that of CHOL (8.7), i.e., 25HC is not as hydrophobic as CHOL. However, it is important to highlight that the hydrophobicity of a molecule does not give any indication about its location, orientation and interactions inside the membrane. Moreover, 25HC might modify the membrane physical properties and therefore modify its interaction with other biological molecules, especially proteins, that could explain its biological properties. As commented above, the only difference between 25HC and CHOL is the addition of a hydroxyl group in carbon C25. This, in principle, simple addition to CHOL should not significantly affect the properties of the phospholipid matrix compared to the parent molecule but must lead to a significant change in the global properties of the membrane since it introduces a polar group capable of hydrogen bonding in the most hydrophobic part of the membrane palisade structure. There should be no strong preferences for the head or tail of 25HC to point towards the water solvent but it should increase its interaction with membrane lipids, with CHOL/25HC molecules, speed up the flip-flop process, induce aggregation, etc., leading to a change in the membrane biophysical properties [33]. In fact, it has been described that 25HC disorders lipid membranes, expands the membrane and reduces membrane thickness [30]. 25HC could retain the orientation that CHOL has in the membrane or could even have an inverted orientation relative to it, i.e., with the steroid ring near the centre of the bilayer and the hydroxyl group at carbon C25 near the phospholipid interphase. Indeed, it has been recently suggested that 25HC could possess both different orientations in the membrane [34,35]. However, the preference seems to be higher for the molecule having its C3 hydroxyl group anchored to the membrane interphase than its C25 counterpart [35]. It has also been proposed that both hydroxyl groups of 25HC would be located at the membrane interface, near the phospholipid head-groups [36] but such 25HC orientation should greatly affect the physical properties of the membrane. Therefore, it can be inferred that 25HC can affect the biological membrane or interact with cellular proteins or both, but it is clear that a general and common mechanism is at play. Though the precise mechanism of the broad antiviral action of 25HC is far from been understood, the existence of a general and common mechanism points out to the biological membrane as its main target.

Molecular dynamics (MD) is a very convenient methodology to explore the dynamics, location, interaction and structure of many different types of molecules inside biological model membranes [37]. The fact that the 25HC mode of action could be through modulation of the membrane properties, it seems reasonable to reason that the biological mode of action of 25HC might be attributed to its interactions with lipid molecules, its effect on the membrane general structure, and, last but not least, its location and orientation in the membrane. In this study, we have used atomistic MD to define the location and orientation of 25HC in the membrane and at the same time to determine the presence of any interactions with membrane phospholipids and CHOL. Trying to get as close as possible to reality, we have studied two different model biomembrane systems, one of them similar to the lipid composition of the plasma membrane (PM) and the other one to the late endosome membrane (LEM). We have studied four other systems, two PM-derived and two LEM-derived, containing different CHOL/25HC relationships (Table 1) so in total we have studied six membrane complex systems. Our results support that 25HC 1) tends to be primarily oriented perpendicular to the membrane surface, 2) tends to aggregate through hydrogen bonding with each other, even 25HC molecules pertaining to different leaflets, and 3) does not aggregate with CHOL or other lipids. Surprisingly, one of the 25HC molecules was observed to rotate during the molecular dynamics simulation so that its hydroxyl groups exchanged positions, i.e., the hydroxyl group at the C3 carbon was nearer the centre of the bilayer and the hydroxyl group at the C25 carbon was nearer to the phospholipid interphase. Our data suggest that the broad antiviral properties of 25HC could be ascribed to its membranotropic effects and consequently through modulation of the biophysical membrane properties.

2. Materials and methods

Unrestrained all-atom MD simulations were obtained using NAMD 2.13 [38] with the CHARMM36 force field for the protein and the lipids and the CHARMM general force field for 25HC [39–41]. All other MD parameters have been described previously [42]. To remove unfavourable atomic contacts, the membrane model systems were

Table 1
Systems and number of components used in this study. The NaCl concentration was 0.15 M. The production trajectories for each one of the six different systems were calculated for 555 ns.

	Systems					
	Late endosome membrane			Plasma membrane		
	LEM_0	LEM_12	LEM_24	PM_0	PM_24	PM_48
POPC	160	160	160	180	180	180
POPE	80	80	80	40	40	40
PI-3P	20	20	20	–	–	–
POPS	–	–	–	20	20	20
BMP	60	60	60	–	–	–
CHOL	80	68	56	160	136	112
25HC	–	12	24	–	24	48
H_2O	28,904	28,902	28,924	28,157	28,164	28,173
Na^+	202	202	202	99	99	99
Cl^-	82	82	82	79	79	79
Dimensions x/y/z (Å)	120/120/114			116/116/114		
PL:CHOL:25HC	80:20:0	80:17:3	80:14:6	30:20:0	30:17:3	30:14:6
CHOL/25HC	–	5.66	2.33	–	5.66	2.33

equilibrated for 1 ns after 100,000 steps of minimization. The production trajectories for each one of the six different systems were run for a total of 555 ns.

Two membrane models systems have been studied, one similar to the plasma membrane (PM) membrane and the other the late endosome (LEM) membrane (Table 1). The PM system without 25HC contained 180 1-palmitoyl-2-oleoyl-sn-glycero-3-phosphocholine (POPC) molecules, 40 of 1-palmitoyl-2-oleoyl-sn-glycero-3-phosphoethanolamine (POPE), 20 of 1-palmitoyl-2-oleoyl-sn-glycero-3-phosphoserine (POPS) and 160 of cholesterol (CHOL) (molar ratio of 9:2:1:8) [26]. The LEM system without 25HC contained 160 POPC molecules, 80 of POPE, 20 of 1-palmitoyl-2-oleoyl-sn-glycero-3-phosphoinositol-3-phosphate (PI-3P), 60 of bis(monoacylglycero)phosphate (BMP) and 80 of CHOL (molar ratio of 8:4:1:3:4) [26] (Table 1). See Supplementary Fig. 1 for the structure of each one of the lipids. Each model system contained 400 lipid molecules (200 lipid molecules in each leaflet) in a rectangular box. Both PM and LEM systems were surrounded by more than 28,000 molecules of water (the solvent-to-lipid ratio was always greater than 70) (cf. Table 1). These ratios represent an excess of water in the membrane systems [43]. The bilayer normal was parallel to the z-axis. At the beginning, the simulation boxes for the PM and LEM systems had the dimensions of 11.6/11.6/11.4 nm and 12/12/11.4 nm, respectively, in the x/y/z directions. Both the height of the simulation box and the cross sectional area were permitted to fluctuate independently of each other. The initial layouts at $t = 0$ ns are depicted in Fig. 1 for both LEM and PM systems. The molecule of 25HC was generated and minimized using Discovery Studio 4.0 (Accelrys Inc., San Diego, USA). The CHARMM General Force Field (CGenFF) compatible stream files of 25HC, which contained the optimized parameter and topology data, were obtained using the Charmm-Gui web server (http://www.charmm-gui.org, [44]). The hydrocarbon chains of the phospholipids were specifically chosen, since the presence of the oleoyl chains increase the overall mobility of the hydrocarbon chains and hence increase the fluidity in the x-y plane of the membrane systems. It should be taken into account that both PM and LEM systems, although having a similar phospholipid composition to the original biological membranes, are an approximation to them, since they do not reflect the hydrocarbon heterogeneity of a biological membrane, lack leaflet composition asymmetry and lack sphingolipids. The LEM and PM membrane models were prepared using the Charmm-Gui web server (http://www.charmm-gui.org, [44]). The membrane model systems were first generated without including the molecule of 25HC (Fig. 1). Afterwards, CHOL molecules were randomly replaced with 25HC to obtain the desired CHOL/25HC ratios (Fig. 1). All 25HC molecules were oriented initially in the standard cholesterol orientation, i.e., the C3 carbon close to the water interface. The simulations were run under an electrostatically neutral environment with an appropriate number of chloride and sodium ions to reach 0.15 M NaCl in the systems, i.e., physiological conditions (Table 1).

The surface of the membrane was defined by the average layer of the phosphate atoms of the lipid head-groups and were oriented parallel to the x-y plane. VMD [45] was used for analysis and visualization. The radial distribution function (with a resolution of 0.1 Å) and the number of molecular contacts were obtained using standard VMD plugins. S_{CD} order parameters, membrane thickness, molecular areas, centre-of-masses and molecule tilt were calculated as previously described [42] using VMD "Membplugin" [46]. Mass density profiles were calculated using the VMD "Density Profile Tool" plugin [47]. The surface area per lipid was calculated as previously described [42]. The orientation of 25HC and CHOL relative to the membrane was measured by the angle defined by the vector defined by carbons C3 and C17 of the molecules of 25HC/CHOL and the z-axis of the membrane (see Supplementary Fig. 1F and G for numbering). The conditions used to determine the presence of a hydrogen bond were a distance less than 2.5 Å between donor and acceptor heavy atoms and a donor-H-acceptor angle of at least 150° [48]. The study was made over the entire MD simulation except where noted.

3. Results and discussion

3.1. Membrane equilibration

To assess the suitability of the simulation methodology and to evaluate the equilibration of the membrane systems, we studied the time variation of the area per lipid for all the lipids in the systems [49,50]. The time plots of the average molecular area for all the lipids in both types of systems are shown in Fig. 2. The molecular areas of POPC, POPE, PI-3P, BMP, CHOL and 25HC for the systems LEM0, LEM12 and LEM24 are shown in Fig. 2A–C, respectively, whereas the molecular areas of POPC, POPE, POPS, CHOL and 25HC for the systems PM0, PM12 and PM24 are shown in Fig. 2D–F, respectively. The data indicate that CHOL, 25HC and the phospholipids were equilibrated relatively early on the course of the simulation showing that the membrane system reached a steady state after ~25–30 ns of simulation. For the last 30 ns of the simulation, the average area of all the lipids are shown in Supplementary Table 1. Those values are comparable to those previously reported [42,51,52]. The molecular areas of POPC, POPE, PI-3P and POPS in the different systems are very similar to each other. However, it is remarkable to emphasize the differences in variability of the molecular areas pertaining to CHOL and 25HC, much higher for the later than for the former, which would imply that the 25HC molecule oscillates in the membrane more than CHOL (Fig. 2B–C and E–F).

Similarly, the average distance between the phosphate atoms of the phospholipids and the oxygen O3 atoms of CHOL and 25HC of opposite leaflets, remained practically constant after ~30–35 ns of the simulation time stressing the fact that the systems were equilibrated after that time (Supplementary Fig. 2). These values were similar to those previously reported for other systems containing CHOL (i.e., the system POPC/PSM/CHOL presented a bilayer thickness of ~46 Å for [51]). Interestingly, the fluctuation of the phospholipids along the whole simulation for all systems is slightly higher than for the CHOL and 25HC, which would imply that the movement variation of the phospholipids along the z-axis is greater than those of CHOL and 25HC. At the same time, the fluctuation of 25HC is greater than that one of CHOL, which also correlates with the greater fluctuation in molecular area of 25HC noted above. Similarly, the fluctuation along the z-axis is also higher for the LEM system than for the PM one. The average distance values for the last 30 ns are shown in Supplementary Table 1 and Supplementary Fig. 2G. The values for all the lipids are higher for the PM system than for the LEM system by about 3 Å [42]. Interestingly, BMP seems to induce the phospholipids in the LEM system to have a larger molecular area than in the PM one but a lower thickness for the same phospholipids in the LEM system respect the PM one. These differences should originate from the different lipid packing in both membrane systems and demonstrate the presence of significant differences in location and structure for the phospholipids in both LEM and PM membrane systems.

In order to check the behaviour of all lipid molecules in the membrane throughout the simulation, we have determined the variation of the centre-of-mass of their representative atoms, phosphates for phospholipids and oxygens for CHOL and 25HC (Fig. 3A–F). At first glance, the centre-of-masses of the different atoms remained reasonably stable after ~30–35 ns of the simulation time so that all the systems were equilibrated after that time as well as the movement variation of 25HC along the z-axis is greater than CHOL. The data also shows that all molecules, except one (see below), maintain their position along the whole simulation without any flip-flop between the two leaflets or changing their orientation in the leaflet where they are. However, one of the 25HC residues (residue no. 6 in the LEM24 system) changed its orientation at the leaflet it was present, but not from one leaflet to the other, at the beginning of the simulation (Fig. 3G). The change in orientation was a relatively slow one, since it flipped from one orientation to the other in about 140 ns (Fig. 3H). Interestingly, the molecule

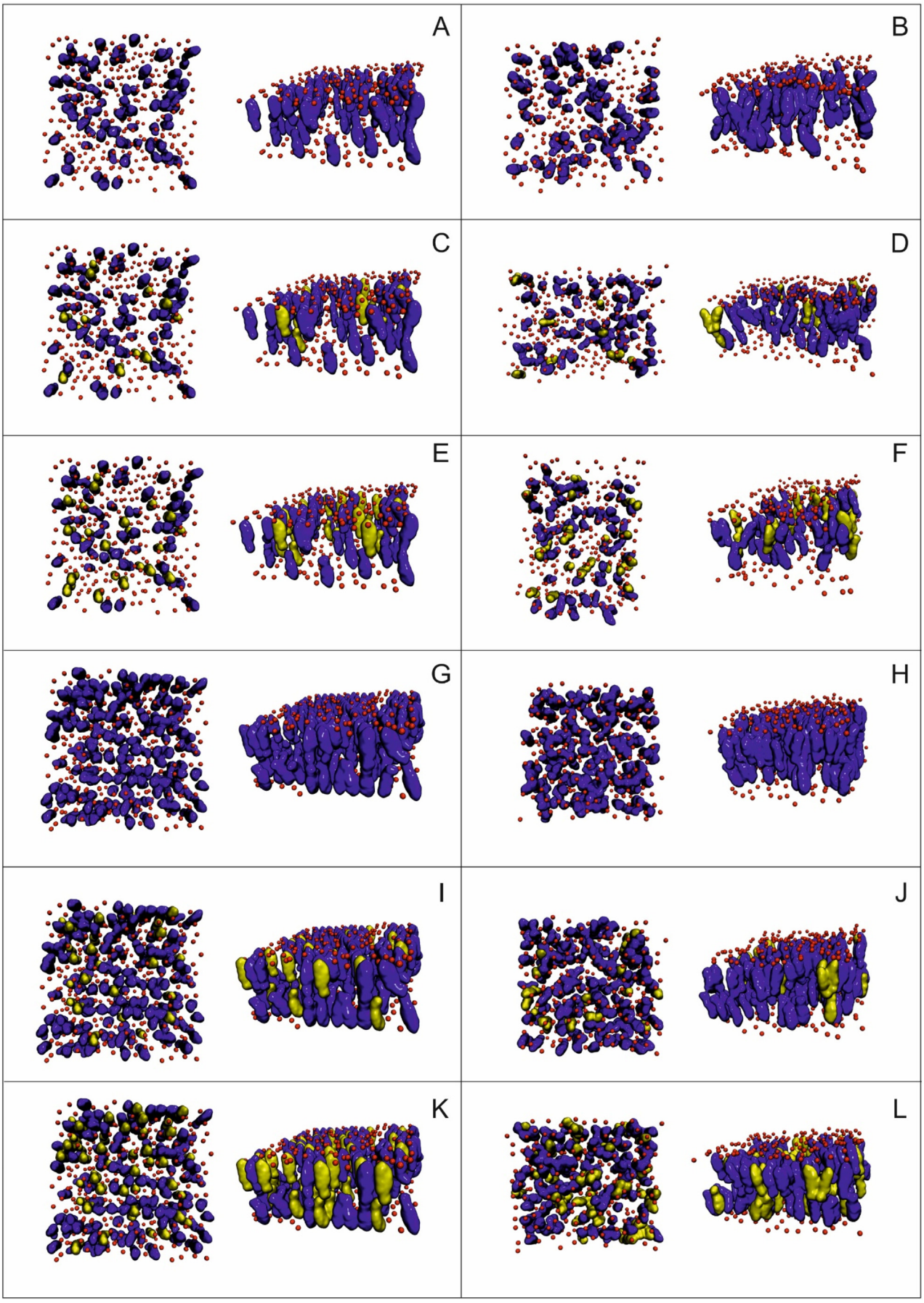

(caption on next page)

Fig. 1. The initial (t = 0 ns, A, C, E, G, I, K) and final (t = 555 ns, B, D, F, H, J, L) layouts of the PM and LEM systems in apical and perspective representation: (A, B) LEM0, (C, D) LEM12, (E, F) LEM24, (G, H) PM0, (I, J) PM24 and (K, L) PM48. The phosphate atoms of the phospholipids, defining the upper and lower boundaries of the membrane, are depicted in VDW representation and red colour. The phosphate atoms clearly define the boundary between the exterior and interior part of the membrane. 25HC and CHOL molecules are depicted in surface representation, yellow and blue, respectively. Phospholipid and water molecules as well as sodium and chloride atoms have been removed for clarity. (For interpretation of the references to colour in this figure legend, the reader is referred to the web version of this article.)

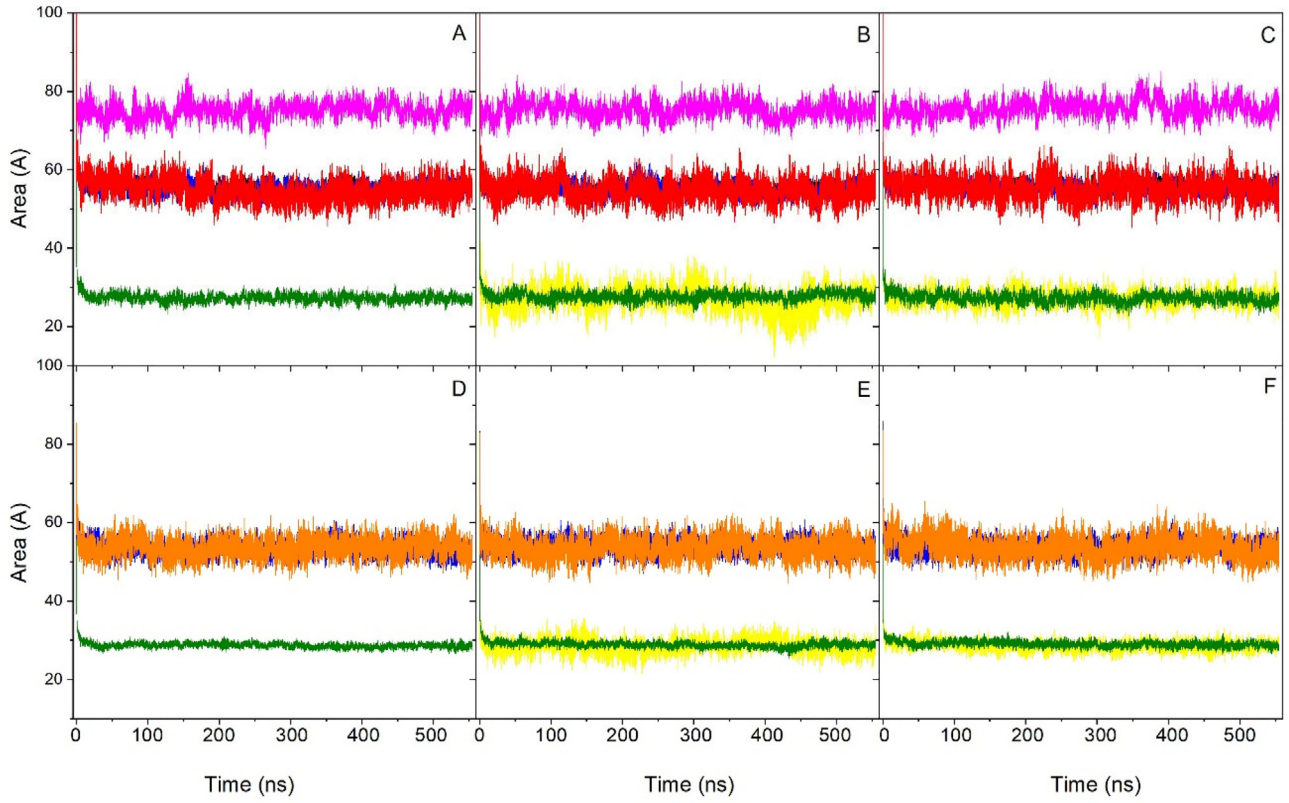

Fig. 2. Time variation of the molecular areas for the whole simulation time for each lipid species in the (A) LEM0, (B) LEM12, (C) LEM24, (D) PM0, (E) PM24 and (F) PM48 membrane model systems. The following lipids are depicted: POPC (black), POPE (blue), POPS (orange), PI-3P (red), BMP (magenta), CHOL (olive) and 25HC (yellow). (For interpretation of the references to colour in this figure legend, the reader is referred to the web version of this article.)

remained parallel to the membrane surface in the central part of the palisade structure of the membrane for about 20 ns. Since the longest distance from oxygens O3 and O25 of 25HC is 16.1 Å and this distance was never reached for any of the 25HC molecules, including residue 6 of the LEM24 system, 25HC were either inclined with respect to the membrane surface or the side chain was not completely extended or both. Considering the specific structure of 25HC, i.e., that it does have a tetracyclic ring and a side chain, it does not completely span one membrane monolayer and that the distance between its oxygens O3 and O24 in its most extended configuration is 16.1 Å, 25HC location inside the membrane is similar to that of CHOL and is tilted with respect to the membrane perpendicular (see below).

3.2. Membrane mass density profiles

The average last 30 ns of the simulation mass density profiles for all the lipids in both LEM and PM membrane model systems are shown in Supplementary Fig. 4. All of the profiles are reasonably symmetric between the two leaflets of the membrane, implying a similar behaviour for all the lipids inside it. By comparing the mass density profiles between both LEM (Supplementary Fig. 4A, C, and D) and PM systems (Supplementary Fig. 4G, I, and L), it is interesting to highlight that the profiles from the later system are much more wide-spread than those of the previous one, and this description applies to all the lipids in each system. The increased bandwidth of the mass density profiles of the lipids would indicate a similar position but slightly different orientation and/or movement inside the leaflets. This difference in behaviour should be ascribed to a greater rocking of the lipids in the LEM systems than in the PM ones and this difference would probably be due to the presence of the BMP phospholipid in the former one. As previously commented, BMP is unique and with a relatively high concentration in late endosomes [26,27] and BMP, due to its particular structure, is a cone-shaped lipid, i.e., a lipid with negative spontaneous curvature [53]. Therefore, BMP has the capacity to modify the curvature of the membrane and strain it [54]. Due to these properties of BMP, the average width of the membrane is 3 Å larger in the PM system than in the LEM one (Supp. Fig. 4B, D and F for the LEM systems and Supp. Fig. 4H, J and L for the PM systems, respectively). With respect to CHOL and 25HC, it can be said that, although both of them share a similar depth in the membrane, their position is not identical, (Supp. Fig. 4D and F and Supp. Fig. 4J and L, respectively). After obtaining the second derivative of the curves (not shown for briefness), the O3 atom of 25HC is roughly 1 Å lower than the O3 of CHOL for all the samples containing both types of molecules, implying that either the 25HC position in the membrane is slightly lower or 25HC is more tilted or both than CHOL (see below).

3.3. 25HC orientation in the membrane

As noted above, 25HC molecules seem to be more tilted than CHOL

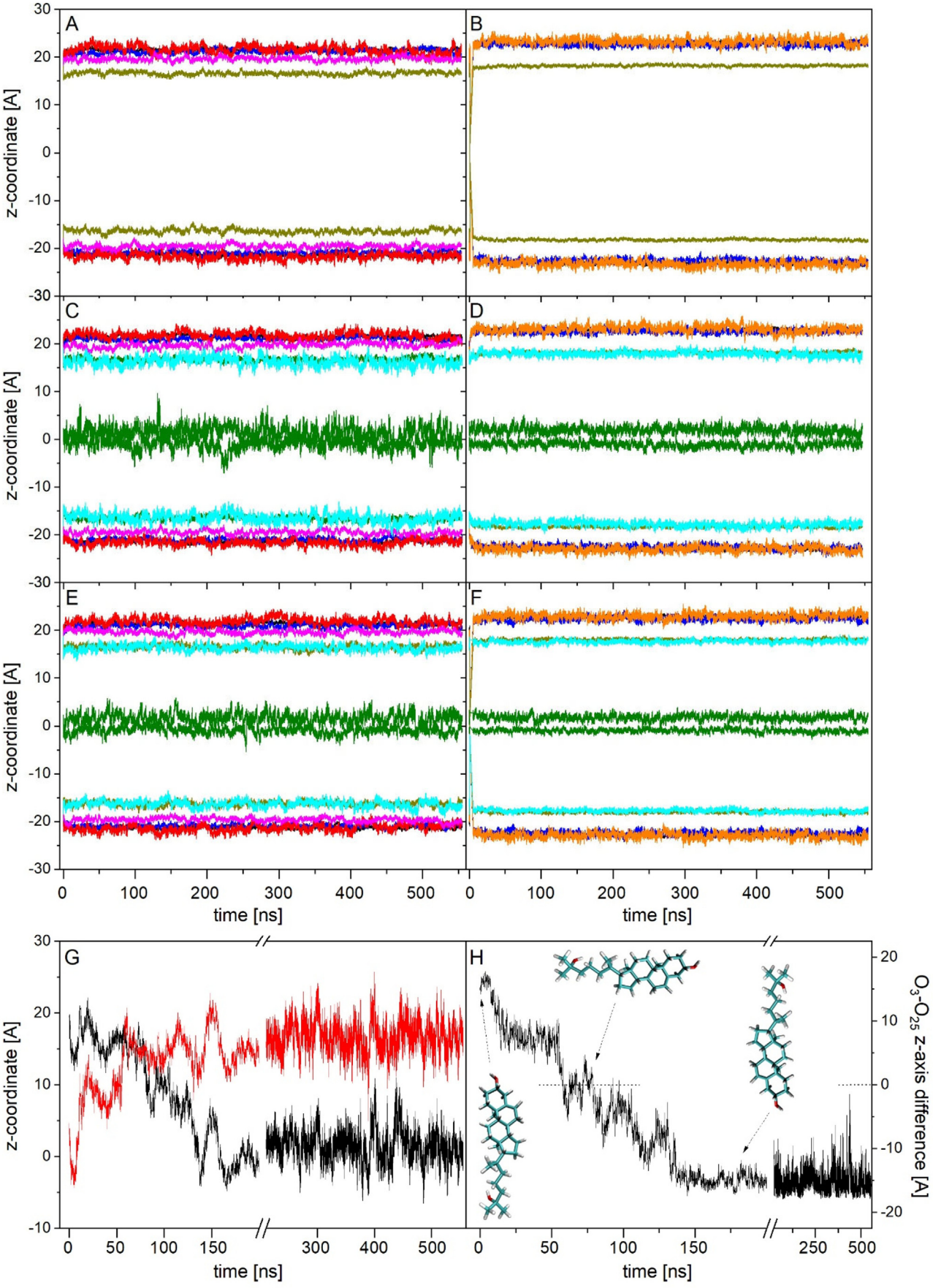

(caption on next page)

Fig. 3. Time variation of the centre-of-mass for the phosphate atoms of the phospholipids and the oxygens of CHOL and 25HC molecules for each one of the lipid types in the (a) LEM0, (c) LEM12, (e) LEM24, (b) PM0, (d) PM24 and (f) PM48 systems. POPC, POPE, POPS, PI-3P, BMP and CHOL are drawn in black (—), blue (—), orange (—), red (—), magenta (—) and dark yellow (—), respectively. 25HC O3 and O25 oxygens are drawn in cyan (—) and olive (—), respectively. For the system LEM24 shown in (E), data for 25HC correspond to residues 1–5 and 7–24. The centre-of-mass of the O3 (black, —) and O25 (red, —) oxygen atoms pertaining to the 25HC residue no. 6 of system LEM24 are shown in (G). The z-axis distance difference between the O3 and O25 oxygen atoms of the LEM24 25HC residue no. 6 is shown in (H). (For interpretation of the references to colour in this figure legend, the reader is referred to the web version of this article.)

in both LEM and PM membrane systems. To verify the 25HC orientation, the orientations of both 25HC and CHOL molecules in the membrane were studied considering the angle formed by the molecular axis defined by the vector joining carbons C3 and C17 of both molecules and the membrane z-axis (Supplementary Fig. 1). The tilt angle histograms of these molecules for the last 30 ns of the molecular dynamics simulation are shown in Fig. 4. The average tilt angle of CHOL in the LEM0 and PM0 systems, i.e., without 25HC, were 160.2 ± 1.3° and 168 ± 0.8°, respectively (180° being completely perpendicular to the membrane surface, the O3 oxygen towards the membrane surface) (Fig. 4A and D). It should be remembered that there are 80 and 160 molecules of CHOL in the LEM0 and PM0 systems, respectively, and the data shown here represent the average over all those molecules. The average tilt angle of CHOL in the LEM12 and LEM24 systems were 160.6 ± 1.6° and 160.1 ± 1.5°, respectively (Fig. 4B), whereas the average tilt angle of 25HC in the LEM12 and LEM24 systems were 158.3 ± 2.9° and 153.5 ± 2.1°, respectively (Fig. 4C). The average CHOL tilting in the LEM systems was very similar in all of them, regardless of the 25HC concentration. However, the 25HC tilting orientation was lower than CHOL in both LEM12 and LEM24 systems, about 6° lower in the later system, where the 25HC concentration was greater. The average tilt angle of CHOL in the PM24 and PM48 systems were 167 ± 0.7° and 166.9 ± 0.8°, respectively (Fig. 4E), whereas the average tilt angle of 25HC in the PM24 and PM48 systems were 167.1 ± 1.3° and 166.4 ± 1°, respectively (Fig. 4F). The tilting angle of CHOL in both PM24 and PM48 systems was therefore identical to the PM0 system, so that the 25HC presence has no effect on the tilting angle of CHOL. Interestingly, the tilting angle of 25HC also was identical to the CHOL average orientation, showing that both CHOL and 25HC were identical in membrane orientation in all PM systems (but not in the LEM ones). As observed in Fig. 4G and H, the average orientation of 25HC and CHOL in the LEM and PM systems is an oblique one, much more tilted in the former than in the later. These values again reinforce the different behaviour of 25HC and CHOL in both LEM and PM membrane model systems: similar in the PM system but different in the LEM one. This behaviour should be related to the spread on the density profiles observed in the LEM systems compared to the PM ones (Supplementary Fig. 4).

3.4. 25HC behaviour

It is interesting to compare the distribution of 25HC at the beginning and at the end of the MD simulation (Fig. 1C and D for LEM12, Fig. 1E and F for LEM24, Fig. 1I and J for PM24 and Fig. 1K and L for PM48). As it was commented above, at the beginning of the simulation in both PM and LEM model systems the 25HC molecules were positioned randomly inside the membrane substituting CHOL molecules at their same positions but without touching each other, i.e., at the beginning no 25HC were next to another 25HC molecule in each system. However, at the end of the simulation, many of the 25HC molecules were forming dimers, trimers and tetramers, both in the same leaflet and in between the two leaflets (Fig. 1).

We have studied the number of 25HC molecules that are within 7 Å of each other and have any contacts between them in the course of the last 30 ns of the simulation time and the results are summarized in Supplementary Table 2. The number of 25HC molecules that present a significant number of contacts are significant and it can be observed that the more number of 25HC molecules in the system, the more molecules having contacts between them are observed. From the data shown in Supplementary Table 2, i.e., 25HC residue numbers of those molecules in contact between them, two interesting facts can be inferred. The first one is that there are different degrees of "aggregation" between 25HC, since it can be observed that there are dimers, trimers, tetramers and higher aggregated numbers, being the dimers and trimers the more abundant aggregation numbers. The second one, is that the aggregation 25HC does not occur only in one of the leaflets but in both of them, so that we can find aggregates of 25HC pertaining to different leaflets. Significantly, those 25HC that are contacting each other and pertaining to different leaflets are joined by interactions between their oxygen atoms at carbon C25.

We have also calculated the average normalized number of hydrogen bonds between each and every one of the 25HC molecules in the course of the last 30 ns of the simulation time and the results are summarized in Supplementary Table 2. Similarly to what was shown above, the number of 25HC molecules that present hydrogen bonding are significant and, likewise, the more number of 25HC in the system, the more molecules having hydrogen bonding between them are observed. From the data presented in Supplementary Table 2, it can be observed that the residue numbers of those 25HC presenting hydrogen bonding is nearly identical to those molecules presenting contacts between them (see above). 25HC molecules located in the same leaflet and in both leaflets may present hydrogen bonding between them. It should be noted that contact values can be obtained from any contact between all atoms of the molecules but hydrogen bonding can occur only through oxygen atoms at carbons C3 and C25. Nevertheless, percentage data from contacts and hydrogen bonding are nearly identical. We have determined the average number of hydrogen bonds per 25HC pair in aggregated form for the last 30 ns of simulation time and the values obtained are: 0.57 ± 0.24 for the lem12 system, 0.76 ± 0.34 for the lem24 system, 0.60 ± 0.26 for the pm24 system and 0.79 ± 0.30 for the pm48 system. The average number of hydrogen bonds per 25HC pair in non-aggregated form, per CHOL pair and per 25HC/CHOL pairs are practically zero, i.e., non-existent. These data demonstrate the presence of a specific interaction between different 25HC molecules in the membrane but not with CHOL. The percentage of 25HC interacting between each other is shown in Supplementary Table 2. The percentage values also show that the interaction between different 25HC molecules are independent of the membrane system, since interaction percentages are very similar between the LEM and PM systems (Supplementary Table 2).

As noted above, 25HC residue no. 6 in the LEM24 system changed its orientation at the leaflet it was present and flipped 180°, its rings pointing towards the centre of the bilayer. This residue always remained at the upper leaflet. Interestingly, this residue formed a trimer with 25HC residues no. 14 and 19 (Supplementary Table 2 and Supplementary Fig. 5). It can be observed in Supplementary Fig. 5 the structure of the trimer they form, where it can be seen the arrangement of the molecules, so that their OH groups are in close contact. For residue no. 6, the OH group involved in binding is the O3 atom, whereas for residues 14 and 19 are the O25 oxygen atoms. Since 25HC molecule no. 6 in the LEM24 system is the only one which has been found to rotate 180°, all other 25HC molecules form aggregates though their O25 oxygen atoms.

We have obtained the radial distribution function, g(r), for each of the lipid molecules in the different systems in order to ascertain the probability of locating each lipid in relation to 25HC (Supplementary

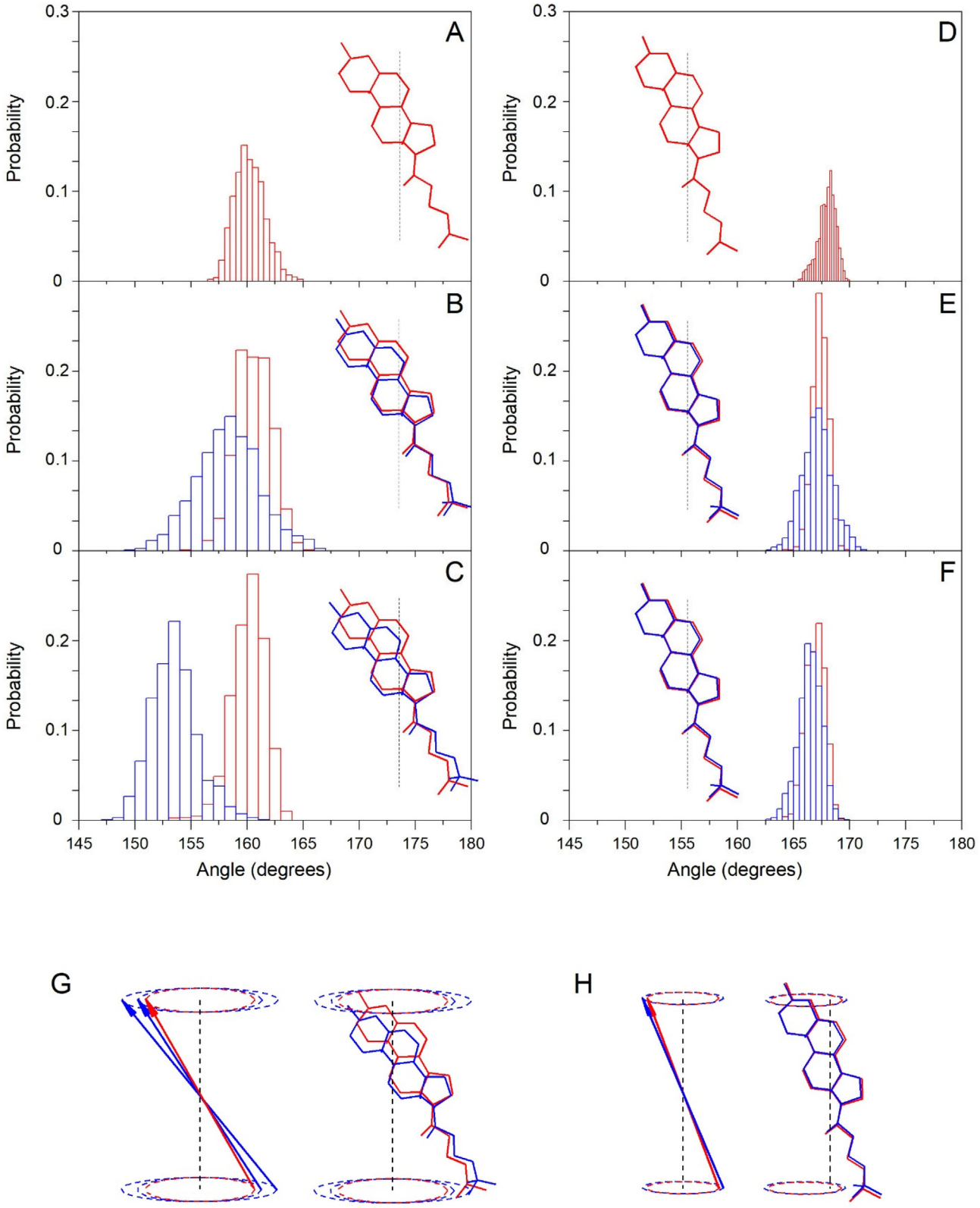

Fig. 4. Tilt angle histograms corresponding to the last 30 ns of the molecular dynamics simulation for the 25HC (blue) and CHOL (red) molecules with respect to the perpendicular of the membrane surface for the (A) LEM0, (B) LEM12, (C) LEM24, (D) PM0, (E) PM24 and (F) PM48 late endosome (panels A, B and C) and plasma (panels D, E and F) membrane model systems. Panels G and H present the combination of all data for the late endosome and plasma membrane model systems, respectively. The tilt angle is defined by the vector joining the membrane z-axis and carbons C3 and C17 of both 25HC and CHOL. (For interpretation of the references to colour in this figure legend, the reader is referred to the web version of this article.)

Fig. 6). For both the LEM12 and LEM24 systems and for the *first* 30 ns of simulation, the most intense signals originated from both BMP and CHOL (Supplementary Fig. 6A and C). For BMP and CHOL in the LEM12 system the highest g(r) values appear at about 6.7 Å and 7.6 Å, respectively, whereas in the LEM24 system the highest g(r) values appear at about 7.9 Å and 7.3 Å, respectively. For the *last* 30 ns of simulation, the most intense signal originates from CHOL for both LEM12 and LEM24 systems: for the LEM12 system, the highest g(r) value of CHOL appears at about 6.7 Å (Supplementary Fig. 6B), whereas for the LEM24 system the highest g(r) value appears at about 7.5 Å (Supplementary Fig. 6D). As observed in the figures, the signals corresponding to the other lipids are smaller than those from CHOL. For both the PM24 and PM48 systems and for the *first* 30 ns of simulation, the most intense signals originated from CHOL (Supplementary Fig. 6E and G). For CHOL in the PM24 system the highest g(r) value appear at about 7.3 Å, whereas in the PM48 system the highest g(r) value appear at about 7.1 Å, respectively. For the *last* 30 ns of simulation, the most intense signal for the PM24 system originates from POPS followed by CHOL (Supplementary Fig. 6F), whereas for the PM48 system it is the opposite, the most intense signal originates from CHOL followed by POPS (Supplementary Fig. 6H). For the PM24 system, the highest g(r) value of POPS appears at about 6.1 Å whereas that of CHOL appears at about 7.1 Å, and for the PM48 system, the highest g(r) value of CHOL appears at about 8.2 Å whereas that of POPS appears at about 10.6 Å. These data indicate that for the LEM12 and LEM24 systems, at the beginning of the simulation, both BMP and CHOL had the highest probability to be found near 25HC. However, at the end of the simulation, CHOL and to a lesser extent the other lipids had the greater probability to be found around 25HC in the membrane. For the PM24 and PM48 systems and at the beginning of the simulation, CHOL and POPS had the highest probability to be found near 25HC; the same probability is maintained until the end of the MD simulation. These data also reveals that 25HC behaves differently in both LEM and PM systems, since it prefers to be surrounded by CHOL in the former system and POPS/CHOL in the later one.

3.5. 25HC/lipid interaction

We have also studied the $-S_{CD}$ order parameters of the phospholipid hydrocarbon chains in the presence and absence of 25HC in order to see differences, if any, in the systems studied in this work (Supplementary Figs. 7–12). The values of the $-S_{CD}$ order parameters give us a clue about the order of the phospholipids in the systems since an $-S_{CD}$ value of 0 designates isotropic orientation, i.e., complete disorder, a value of 0.5 states complete order along the normal bilayer and a value of −0.25 points to full order [55]. For the LEM0 system, system containing 20% CHOL but no 25HC, the average $-S_{CD}$ values of the acyl chains of all phospholipids distant from CHOL, i.e., in the bulk membrane model system, are according to the profiles observed earlier for both simulated and experimental data of systems containing CHOL [41,56,57] (Supplementary Fig. 7). Significantly, the hydrocarbon chain $-S_{CD}$ order parameters of the phospholipid acyl chains near the CHOL molecules were higher than those corresponding to the bulk ones, implicating that the proximity of the phospholipids to the CHOL molecules induced an increase in their order (decrease in fluidity) as it should be (Supplementary Fig. 7). Interestingly, the increase in order parameter was more significant for the PI-3P phospholipid and to a lesser extent also for BMP (Supplementary Fig. 9E–F and Supplementary Fig. 7G–H) compared to both POPC and POPE phospholipids (Supplementary Fig. 7A–B and Supplementary Fig. 9C–D). For the LEM12 system, i.e., system containing 17% CHOL and 3% 25HC, the average $-S_{CD}$ values of the acyl chains of the bulk phospholipids were similar to the profiles observed for the LEM0 system (Supplementary Fig. 8). The hydrocarbon chain $-S_{CD}$ order parameters of the phospholipid acyl chains near the CHOL and 25HC molecules were slightly higher than those corresponding to the bulk ones, indicating that the proximity of the phospholipids to both CHOL and 25HC induced an increase in their order (Supplementary Fig. 8A–H). Interestingly, the $-S_{CD}$ order parameters of the phospholipid acyl chains near CHOL were slightly higher than those near 25HC except for PI-3P, where the order parameters of the phospholipids near 25HC were higher than those near to CHOL (Supplementary Fig. 8E–F). For the LEM24 system, i.e., system containing 14% CHOL and 6% 25HC, the average $-S_{CD}$ values of the acyl chains of the bulk phospholipids were also similar to the profiles observed for the LEM0 system (Supplementary Fig. 9). Similar to what was noted above, the hydrocarbon chain $-S_{CD}$ order parameters of the phospholipid acyl chains near the CHOL and 25HC were slightly higher than those corresponding to the bulk ones, indicating that the proximity of the phospholipids to both CHOL and 25HC induced an increase in their order (Supplementary Fig. 9A–H). In this case, the $-S_{CD}$ order parameters of the phospholipid acyl chains near CHOL were relatively similar to those near 25HC.

For the PM0 system, i.e., system containing 40% CHOL and no 25HC, the mean $-S_{CD}$ values of the acyl chains of all phospholipids distant from CHOL, i.e., in the bulk membrane model system, are comparable to the profiles obtained for both simulated and experimental data of systems containing CHOL [41,56,57] (Supplementary Fig. 10). Interestingly, the $-S_{CD}$ order parameters of the phospholipid acyl chains near the CHOL molecules were very similar to those corresponding to the bulk ones, implicating that at this high percentage of CHOL its induced effects are of long range and similar to all phospholipids present in the system. Unlike the LEM0 system, no differences were found for the distinct phospholipids present in the PM0 system. For the PM24 system, i.e., system containing 34% CHOL and 6% 25HC, the average $-S_{CD}$ values of the acyl chains of the bulk phospholipids were nearly identical to the profiles observed for the PM0 system (Supplementary Fig. 11). In this case, the$-S_{CD}$ order parameters of the phospholipid acyl chains near CHOL and 25HC were very similar to those of the bulk ones and no differences were found between the different phospholipids. For the PM48 system, i.e., system containing 28% CHOL and 12% 25HC, the average $-S_{CD}$ values of the acyl chains of the bulk phospholipids were very similar to the profiles observed for the PM0 and PM24 systems (Supplementary Fig. 12). And similarly to what was observed for the PM24 system, the $-S_{CD}$ order parameters of the phospholipid acyl chains near CHOL and 25HC were very similar to those of the bulk ones and no differences were found between the different phospholipids. In summary, for the LEM systems, i.e., LEM0, LEM12 and LEM24, the order parameters of the phospholipid acyl chains near CHOL and 25HC were slightly higher than those pertaining to the bulk ones, possibly because the CHOL/25HC global percentage in those systems was 20%, i.e., relatively low. However, small differences were found when comparing the order parameters of the phospholipids near CHOL and 25HC, implying that subtle differences might exist between the effects produced by CHOL and 25HC. As for the case of the three PM systems, i.e., PM0, PM24 and PM48, there were no significant differences between the order parameters of the phospholipid acyl chains corresponding to the bulk ones or those phospholipids near CHOL or 25HC. These data would suggest that its effect on the phospholipid order is nearly identical and no differences between CHOL and 25HC exists in the PM systems. These data would reflect the long-range effects produced by both CHOL and 25HC in the membrane and stress that no significant effects on the $-S_{CD}$ order parameters of the phospholipid hydrocarbon chains can be discerned between these two different types of molecules.

4. Conclusions

Many molecules that have hydrophobic and/or amphipathic structures interact not only with proteins but also with membrane lipids [58,59]. The various biological properties of these molecules would indicate that diverse mechanisms are at play, but would also indicate the presence of a common point of convergence, i.e., the biological

membrane. The biological and pharmacological attributes of these molecules, as well as their biomedicinal effects, should be associated to a membrane modulation mechanism [59,60]. 25HC, one of the most important oxysterol molecules derived from CHOL, appears to be directly related to the innate immune system and may be a fundamental weapon used by cells to fight bacterial and viral infections [61]. We have intended in this work to define the location of 25HC in the membrane and the detailed interactions it might have with lipids in the membrane using MD simulations. Furthermore, compare it at the same time with CHOL, its parent molecule. For that aim, we have studied two complex model membranes, one similar to the late endosome membrane, LEM, and the other one to the plasma membrane, PM. Our results support that 25HC is inserted in the membrane in a relative stable and steady location, similar but not identical as CHOL. Furthermore, 25HC fluctuates in the membrane to a much greater degree than CHOL both in the x-y plane and in the z-axis, much more in the LEM system than in the PM one. Remarkably, the effect of 25HC on the phospholipid order parameters are not significantly different from CHOL, being the effects modulated by both molecules nearly identical in the PM system. One of the most notable facts about 25HC is that, in contrast to CHOL, tends to aggregate between the same 25HC molecules, forming dimers, trimers and higher-order aggregates, being the dimers and trimers the more abundant aggregation numbers. Apart from that, these aggregates occur not only on one leaflet, but also between different leaflets. These aggregates form spontaneously through the formation of hydrogen bonds between both oxygen atoms of 25HC, being the formation of hydrogen bonds independent of the system studied, be it the LEM or PM systems. Surprisingly, no contacts or hydrogen bonds are observed between 25HC and CHOL molecules as well as between CHOL molecules themselves at any time. Interestingly, CHOL molecules have higher probability to be found near 25HC molecules than any other phospholipid type in the LEM systems; in contrast, both CHOL and POPS are the molecules with higher probability to be found near 25HC molecules in the PM systems. In this context, the actual concentration of 25HC in the membrane should also be taken into account. Blanc et al. have shown that, upon viral infection, cells produce 25HC in the nM range and present IC_{50} values for 25HC lower than 1 μM [11]. These authors also commented the possibility that the biological 25HC effects could be concentration dependent, i.e., relatively low concentrations of 25HC could involve a direct mode of action (protein) and relatively high concentrations could involve an indirect one (membrane). However, it should not be ruled out that 25HC could function at both levels and at the same time. The relative concentration of 25HC/CHOL that we have used in this work is much higher than that found in the cell membrane, either produced by the cell after viral infection or after exogenous addition. At the same time, it could be possible that the spontaneous 25HC aggregation that we have observed in this work could depend on the concentration of 25HC in the cell membrane. However, and as noted above, the percentage of aggregated 25HC molecules was similar in the four different systems studied here, which would suggest that 25HC aggregation, regardless of absolute concentration, would be significant in the plasma and/or endosomal membranes. Some membrane fusion proteins are known to require CHOL-rich domains for fusion to occur, presumably by giving place to special sites located at the boundaries between CHOL and phospholipids [62]. It would be conceivable that 25HC, by forming high-order aggregates without significantly disturbing the properties of the membrane, would modify those protein interaction zones, similar but not identical to those formed by CHOL. 25HC would modify the way those proteins interact with the membrane, leading to a reduction and/or inhibition on the fusion rate and henceforth forming a true innate antiviral molecule. In that situation, it also could be expected that the hydrogen bond network between the different phospholipids should be completely altered compared to the normal situation, i.e., without 25HC [63]. Therefore, the subtle addition of a hydroxyl group at carbon 25 of CHOL, giving place to 25HC, modifies the interfacial properties of the CHOL molecules and, therefore, leads to the inhibition of membrane fusion. The antiviral effect of 25HC could consequently be attributed to its capacity to modulate the membrane biophysical properties and consequently, molecules, similar to 25HC, which could modify the interfacial properties of the membrane could serve as antiviral molecules. Its broad antiviral effect should point to 25HC or its derivatives as a potential bioactive molecule for the treatment of diverse viral diseases.

Declaration of competing interest

The authors declare that they have no conflict of interest.

Acknowledgements

NAMD was developed by the Theoretical and Computational Biophysics Group in the Beckman Institute for Advanced Science and Technology at the University of Illinois at Urbana-Champaign. We are very grateful to SIATDI, Universidad Miguel Hernández (UMH), for the generous use of the UMH Computer Cluster. This work was not funded by any external or internal funding agencies.

Appendix A. Supplementary data

Supplementary data to this article can be found online at https://doi.org/10.1016/j.bbamem.2020.183413.

References

[1] O.G. Mouritsen, M.J. Zuckermann, What's so special about cholesterol? Lipids 39 (2004) 1101–1113.
[2] O.G. Mouritsen, L.A. Bagatolli, Lipid domains in model membranes: a brief historical perspective, Essays Biochem. 57 (2015) 1–19.
[3] W. Kulig, L. Cwiklik, P. Jurkiewicz, T. Rog, I. Vattulainen, Cholesterol oxidation products and their biological importance, Chem. Phys. Lipids 199 (2016) 144–160.
[4] W.J. Griffiths, Y. Wang, An update on oxysterol biochemistry: new discoveries in lipidomics, Biochem. Biophys. Res. Commun. 504 (2018) 617–622.
[5] S.Y. Liu, R. Aliyari, K. Chikere, G. Li, M.D. Marsden, J.K. Smith, O. Pernet, H. Guo, R. Nusbaum, J.A. Zack, A.N. Freiberg, L. Su, B. Lee, G. Cheng, Interferon-inducible cholesterol-25-hydroxylase broadly inhibits viral entry by production of 25-hydroxycholesterol, Immunity 38 (2013) 92–105.
[6] X. Li, P. Hylemon, W.M. Pandak, S. Ren, Enzyme activity assay for cholesterol 27-hydroxylase in mitochondria, J. Lipid Res. 47 (2006) 1507–1512.
[7] T.Y. Chang, C.C. Chang, N. Ohgami, Y. Yamauchi, Cholesterol sensing, trafficking, and esterification, Annu. Rev. Cell Dev. Biol. 22 (2006) 129–157.
[8] U. Diczfalusy, On the formation and possible biological role of 25-hydroxycholesterol, Biochimie 95 (2013) 455–460.
[9] M.E. Abrams, K.A. Johnson, S.S. Perelman, L.S. Zhang, S. Endapally, K.B. Mar, B.M. Thompson, J.G. McDonald, J.W. Schoggins, A. Radhakrishnan, N.M. Alto, Oxysterols provide innate immunity to bacterial infection by mobilizing cell surface accessible cholesterol, Nat. Microbiol. 5 (7) (2020) 929–942, https://doi.org/10.1038/s41564-020-0701-5.
[10] A.A. Kandutsch, H.W. Chen, H.J. Heiniger, Biological activity of some oxygenated sterols, Science 201 (1978) 498–501.
[11] M. Blanc, W.Y. Hsieh, K.A. Robertson, K.A. Kropp, T. Forster, G. Shui, P. Lacaze, S. Watterson, S.J. Griffiths, N.J. Spann, A. Meljon, S. Talbot, K. Krishnan, D.F. Covey, M.R. Wenk, M. Craigon, Z. Ruzsics, J. Haas, A. Angulo, W.J. Griffiths, C.K. Glass, Y. Wang, P. Ghazal, The transcription factor STAT-1 couples macrophage synthesis of 25-hydroxycholesterol to the interferon antiviral response, Immunity 38 (2013) 106–118.
[12] A. Civra, M. Colzani, V. Cagno, R. Francese, V. Leoni, G. Aldini, D. Lembo, G. Poli, Modulation of cell proteome by 25-hydroxycholesterol and 27-hydroxycholesterol: a link between cholesterol metabolism and antiviral defense, Free Radic. Biol. Med. 149 (2020) 30–36, https://doi.org/10.1016/j.freeradbiomed.2019.08.031.
[13] D. Lembo, V. Cagno, A. Civra, G. Poli, Oxysterols: an emerging class of broad spectrum antiviral effectors, Mol. Asp. Med. 49 (2016) 23–30.
[14] C. Li, Y.Q. Deng, S. Wang, F. Ma, R. Aliyari, X.Y. Huang, N.N. Zhang, M. Watanabe, H.L. Dong, P. Liu, X.F. Li, Q. Ye, M. Tian, S. Hong, J. Fan, H. Zhao, L. Li, N. Vishlaghi, J.E. Buth, C. Au, Y. Liu, N. Lu, P. Du, F.X. Qin, B. Zhang, D. Gong, X. Dai, R. Sun, B.G. Novitch, Z. Xu, C.F. Qin, G. Cheng, 25-Hydroxycholesterol protects host against Zika virus infection and its associated microcephaly in a mouse model, Immunity 46 (2017) 446–456.
[15] Y. Yuan, Z. Wang, B. Tian, M. Zhou, Z.F. Fu, L. Zhao, Cholesterol 25-hydroxylase suppresses rabies virus infection by inhibiting viral entry, Arch. Virol. 164 (2019) 2963–2974.
[16] G.T. Shawli, O.O. Adeyemi, N.J. Stonehouse, M.R. Herod, The oxysterol 25-hydroxycholesterol inhibits replication of murine norovirus, Viruses 11 (2019).
[17] J.B.C.R. Zang, M.F. Gomez-Castro, Z. Liu, Q. Zeng, H. Zhao, J. Son, P.W. Rothlauf,

G. Hou, S. Bose, X. Wang, M.D. Vahey, T. Kirchhausen, D.H. Fremont, M.S. Diamond, S.P.J. Whelan, S. Ding, Cholesterol 25-Hydroxylase Suppresses SARS-CoV-2 Replication by Blocking Membrane Fusion, bioRxiv, (2020), https://doi.org/10.1101/2020.06.08.141077.
[18] T. Tang, M. Bidon, J.A. Jaimes, G.R. Whittaker, S. Daniel, Coronavirus membrane fusion mechanism offers as a potential target for antiviral development, Antivir. Res. (2020) 104792.
[19] B. Gomes, S. Goncalves, A. Disalvo, A. Hollmann, N.C. Santos, Effect of 25-hydroxycholesterol in viral membrane fusion: insights on HIV inhibition, Biochim. Biophys. Acta Biomembr. 1860 (2018) 1171–1178.
[20] Y. Chen, S. Wang, Z. Yi, H. Tian, R. Aliyari, Y. Li, G. Chen, P. Liu, J. Zhong, X. Chen, P. Du, L. Su, F.X. Qin, H. Deng, G. Cheng, Interferon-inducible cholesterol-25-hydroxylase inhibits hepatitis C virus replication via distinct mechanisms, Sci. Rep. 4 (2014) 7242.
[21] Y. Zhang, L. Wang, X. Huang, S. Wang, Y. Huang, Q. Qin, Fish cholesterol 25-hydroxylase inhibits virus replication via regulating interferon immune response or affecting virus entry, Front. Immunol. 10 (2019) 322.
[22] Z. Song, J. Bai, H. Nauwynck, L. Lin, X. Liu, J. Yu, P. Jiang, 25-Hydroxycholesterol provides antiviral protection against highly pathogenic porcine reproductive and respiratory syndrome virus in swine, Vet. Microbiol. 231 (2019) 63–70.
[23] M. Bello-Perez, A. Falco, B. Novoa, L. Perez, J. Coll, Hydroxycholesterol binds and enhances the anti-viral activities of zebrafish monomeric c-reactive protein isoforms, PLoS One 14 (2019) e0201509.
[24] A. Doms, T. Sanabria, J.N. Hansen, N. Altan-Bonnet, G.H. Holm, 25-Hydroxycholesterol production by the cholesterol-25-hydroxylase interferon-stimulated gene restricts mammalian reovirus infection, J. Virol. 92 (2018).
[25] A. Civra, R. Francese, P. Gamba, G. Testa, V. Cagno, G. Poli, D. Lembo, 25-Hydroxycholesterol and 27-hydroxycholesterol inhibit human rotavirus infection by sequestering viral particles into late endosomes, Redox Biol. 19 (2018) 318–330.
[26] D.L. Esposito, J.B. Nguyen, D.C. DeWitt, E. Rhoades, Y. Modis, Physico-chemical requirements and kinetics of membrane fusion of flavivirus-like particles, J Gen Virol 96 (2015) 1702–1711.
[27] A.M. Nour, Y. Modis, Endosomal vesicles as vehicles for viral genomes, Trends Cell Biol. 24 (2014) 449–454.
[28] J. Gruenberg, Life in the lumen: the multivesicular endosome, Traffic 21 (2020) 76–93.
[29] A. Honda, K. Yamashita, T. Hara, T. Ikegami, T. Miyazaki, M. Shirai, G. Xu, M. Numazawa, Y. Matsuzaki, Highly sensitive quantification of key regulatory oxysterols in biological samples by LC-ESI-MS/MS, J. Lipid Res. 50 (2009) 350–357.
[30] A.A. Bielska, B.N. Olsen, S.E. Gale, L. Mydock-McGrane, K. Krishnan, N.A. Baker, P.H. Schlesinger, D.F. Covey, D.S. Ory, Side-chain oxysterols modulate cholesterol accessibility through membrane remodeling, Biochemistry 53 (2014) 3042–3051.
[31] B.N. Olsen, P.H. Schlesinger, N.A. Baker, Perturbations of membrane structure by cholesterol and cholesterol derivatives are determined by sterol orientation, J. Am. Chem. Soc. 131 (2009) 4854–4865.
[32] T. Cheng, Y. Zhao, X. Li, F. Lin, Y. Xu, X. Zhang, Y. Li, R. Wang, L. Lai, Computation of octanol-water partition coefficients by guiding an additive model with knowledge, J. Chem. Inf. Model. 47 (2007) 2140–2148.
[33] G. Parisio, M.M. Sperotto, A. Ferrarini, Flip-flop of steroids in phospholipid bilayers: effects of the chemical structure on transbilayer diffusion, J. Am. Chem. Soc. 134 (2012) 12198–12208.
[34] H. Takahashi, T. Hoshino, A comparative study of the effects of 7beta-hydroxycholesterol, 25-hydroxycholesterol, and cholesterol on the structural and thermal phase behavior of multilamellar dipalmitoylphosphatidylcholine bilayer vesicles, Chem. Phys. Lipids 227 (2020) 104872.
[35] A. Wnetrzak, A. Chachaj-Brekiesz, J. Kobierski, K. Karwowska, A.D. Petelska, P. Dynarowicz-Latka, Unusual behavior of the bipolar molecule 25-hydroxycholesterol at the air/water Interface-Langmuir monolayer approach complemented with theoretical calculations, J. Phys. Chem. B 124 (2020) 1104–1114.
[36] V.M. Olkkonen, R. Hynynen, Interactions of oxysterols with membranes and proteins, Mol. Asp. Med. 30 (2009) 123–133.
[37] H.I. Ingolfsson, M.N. Melo, F.J. van Eerden, C. Arnarez, C.A. Lopez, T.A. Wassenaar, X. Periole, A.H. de Vries, D.P. Tieleman, S.J. Marrink, Lipid organization of the plasma membrane, J. Am. Chem. Soc. 136 (2014) 14554–14559.
[38] J.C. Phillips, R. Braun, W. Wang, J. Gumbart, E. Tajkhorshid, E. Villa, C. Chipot, R.D. Skeel, L. Kale, K. Schulten, Scalable molecular dynamics with NAMD, J. Comput. Chem. 26 (2005) 1781–1802.
[39] R.B. Best, X. Zhu, J. Shim, P.E. Lopes, J. Mittal, M. Feig, A.D. Mackerell Jr., Optimization of the additive CHARMM all-atom protein force field targeting improved sampling of the backbone phi, psi and side-chain chi(1) and chi(2) dihedral angles, J. Chem. Theory Comput. 8 (2012) 3257–3273.
[40] K. Vanommeslaeghe, E. Hatcher, C. Acharya, S. Kundu, S. Zhong, J. Shim, E. Darian, O. Guvench, P. Lopes, I. Vorobyov, A.D. Mackerell Jr., CHARMM general force field: a force field for drug-like molecules compatible with the CHARMM all-atom additive biological force fields, J. Comput. Chem. 31 (2010) 671–690.
[41] J.B. Klauda, R.M. Venable, J.A. Freites, J.W. O'Connor, D.J. Tobias, C. Mondragon-Ramirez, I. Vorobyov, A.D. MacKerell Jr., R.W. Pastor, Update of the CHARMM all-atom additive force field for lipids: validation on six lipid types, J. Phys. Chem. B 114 (2010) 7830–7843.
[42] J. Villalain, Epigallocatechin-3-gallate location and interaction with late endosomal and plasma membrane model membranes by molecular dynamics, J. Biomol. Struct. Dyn. 37 (2019) 3122–3134.
[43] K. Murzyn, T. Rog, G. Jezierski, Y. Takaoka, M. Pasenkiewicz-Gierula, Effects of phospholipid unsaturation on the membrane/water interface: a molecular simulation study, Biophys. J. 81 (2001) 170–183.
[44] E.L. Wu, X. Cheng, S. Jo, H. Rui, K.C. Song, E.M. Davila-Contreras, Y. Qi, J. Lee, V. Monje-Galvan, R.M. Venable, J.B. Klauda, W. Im, CHARMM-GUI membrane builder toward realistic biological membrane simulations, J. Comput. Chem. 35 (2014) 1997–2004.
[45] W. Humphrey, A. Dalke, K. Schulten, VMD: visual molecular dynamics, J. Mol. Graph. 14 (1996) 33–38 (27-38).
[46] R. Guixa-Gonzalez, I. Rodriguez-Espigares, J.M. Ramirez-Anguita, P. Carrio-Gaspar, H. Martinez-Seara, T. Giorgino, J. Selent, MEMBPLUGIN: studying membrane complexity in VMD, Bioinformatics 30 (2014) 1478–1480.
[47] T. Giorgino, Computing 1-D atomic densities in macromolecular simulations: the density profile tool for VMD, Computer Physics Communication 185 (2014) 317–322.
[48] J.L. Baylon, E. Tajkhorshid, Capturing spontaneous membrane insertion of the influenza virus hemagglutinin fusion peptide, J. Phys. Chem. B 119 (2015) 7882–7893.
[49] C. Kandt, W.L. Ash, D.P. Tieleman, Setting up and running molecular dynamics simulations of membrane proteins, Methods 41 (2007) 475–488.
[50] C. Anézo, A.H. de Vries, H.-D. Höltje, D.P. Tieleman, S.-J. Marrink, Methodological issues in lipid bilayers simulations, J. Phys. Chem. B 107 (2003) 9424–9433.
[51] I. Bera, J.B. Klauda, Molecular simulations of mixed lipid bilayers with sphingomyelin, glycerophospholipids, and cholesterol, J. Phys. Chem. B 121 (2017) 5197–5208.
[52] P. Mukhopadhyay, L. Monticelli, D.P. Tieleman, Molecular dynamics simulation of a palmitoyl-oleoyl phosphatidylserine bilayer with Na+ counterions and NaCl, Biophys. J. 86 (2004) 1601–1609.
[53] E. Zaitseva, S.T. Yang, K. Melikov, S. Pourmal, L.V. Chernomordik, Dengue virus ensures its fusion in late endosomes using compartment-specific lipids, PLoS Pathog. 6 (2010) e1001131.
[54] H. Matsuo, J. Chevallier, N. Mayran, I. Le Blanc, C. Ferguson, J. Faure, N.S. Blanc, S. Matile, J. Dubochet, R. Sadoul, R.G. Parton, F. Vilbois, J. Gruenberg, Role of LBPA and Alix in multivesicular liposome formation and endosome organization, Science 303 (2004) 531–534.
[55] D.P. Tieleman, S.J. Marrink, H.J. Berendsen, A computer perspective of membranes: molecular dynamics studies of lipid bilayer systems, Biochim. Biophys. Acta 1331 (1997) 235–270.
[56] H.H. Tsai, J.B. Lee, H.S. Li, T.Y. Hou, W.Y. Chu, P.C. Shen, Y.Y. Chen, C.J. Tan, J.C. Hu, C.C. Chiu, Geometrical effects of phospholipid olefinic bonds on the structure and dynamics of membranes: a molecular dynamics study, Biochim. Biophys. Acta 1848 (2015) 1234–1247.
[57] R.A. Bockmann, A. Hac, T. Heimburg, H. Grubmuller, Effect of sodium chloride on a lipid bilayer, Biophys. J. 85 (2003) 1647–1655.
[58] W. Kopec, J. Telenius, H. Khandelia, Molecular dynamics simulations of the interactions of medicinal plant extracts and drugs with lipid bilayer membranes, FEBS J. 280 (2013) 2785–2805.
[59] H. Tsuchiya, Membrane interactions of phytochemicals as their molecular mechanism applicable to the discovery of drug leads from plants, Molecules 20 (2015) 18923–18966.
[60] D. Margina, M. Ilie, G. Manda, I. Neagoe, M. Mocanu, D. Ionescu, D. Gradinaru, C. Ganea, Quercetin and epigallocatechin gallate effects on the cell membranes biophysical properties correlate with their antioxidant potential, Gen. Physiol. Biophys. 31 (2012) 47–55.
[61] (!!! INVALID CITATION !!! [5, 7-16]).
[62] J. Fantini, R.M. Epand, F.J. Barrantes, Cholesterol-recognition motifs in membrane proteins, Adv. Exp. Med. Biol. 1135 (2019) 3–25.
[63] X. Zhuang, E.M. Davila-Contreras, A.H. Beaven, W. Im, J.B. Klauda, An extensive simulation study of lipid bilayer properties with different head groups, acyl chain lengths, and chain saturations, Biochim. Biophys. Acta 1858 (2016) 3093–3104.